Structure-function relationship of biological gels revealed by multiple-particle tracking and differential interference contrast microscopy: The case of human lamin networks

Porntula Panorchan,[1] Denis Wirtz,[1,2] and Yiider Tseng[1,*]
[1]*Department of Chemical and Biomolecular Engineering, The Johns Hopkins University, 3400 North Charles Street, Baltimore, Maryland 21218, USA*
[2]*Department of Materials Science and Engineering, The Johns Hopkins University, 3400 North Charles Street, Baltimore, Maryland 21218, USA*
(Received 3 May 2004; published 27 October 2004)

Lamin *B*1 filaments organize into a thin dense meshwork underlying the nucleoplasmic side of the nuclear envelope. Recent experiments *in vivo* suggest that lamin *B*1 plays a key structural role in the nuclear envelope, but the intrinsic mechanical properties of lamin *B*1 networks remain unknown. To assess the potential mechanical contribution of lamin *B*1 in maintaining the integrity and providing structural support to the nucleus, we measured the micromechanical properties and examined the ultrastructural distribution of lamin *B*1 networks *in vitro* using particle tracking methods and differential interference contrast (DIC) microscopy. We exploit various surface chemistries of the probe microspheres (carboxylated, polyethylene glycol-coated, and amine-modified) to differentiate lamin-rich from lamin-poor regions and to rigorously extract local viscoelastic moduli from the mean-squared displacements of noninteracting particles. Our results show that human lamin *B*1 can, even in the absence of auxiliary proteins, form stiff and yet extremely porous networks that are well suited to provide structural strength to the nuclear lamina. Combining DIC microscopy and particle tracking allows us to relate directly the local organization of a material to its local mechanical properties, a general methodology that can be extended to living cells.

DOI: 10.1103/PhysRevE.70.041906 PACS number(s): 87.16.−b, 61.25.Hq, 61.41.+e

I. INTRODUCTION

The nuclear lamina is a filamentous meshwork underlying the nucleoplasmic side of the nuclear membrane [1]. The primary components of the nuclear lamina are lamins. Nuclear lamins are type-V intermediate filaments (IF) that share structural features with those of cytoplasmic IF. Nuclear lamins are divided into two categories, *A*-type or *B*-type, based on their original genes. In human cells, through gene splicing, *A*-type lamins are broken down into lamin *A*, *C*, and Δ*NLA* isotypes; *B*-type lamins are broken down into lamin *B*1 and *B*2 isotypes. Nuclear lamins feature a rod-shaped domain consisting of heptad repeats flanked with nonhelical *N*-terminal and *C*-terminal domains. The rod domain plays a critical role in lamin-lamin interactions, both in dimers and higher-order lamin assembly [2,3]. Nuclear lamins, in particular lamin *B*1, are constitutively expressed [4,5], and involved in the structural maintenance of the nuclear envelope [6,7], which may play a scaffolding role for chromatin [8].

In vitro assembly of lamins has been studied extensively using proteins purified from either animal tissues or recombinant lamin [1,2,9–12]. Lamin monomers form parallel, unstaggered, two-stranded dimers via the association of the heptad repeats of the rod domain. These dimers assemble into head-to-tail polymers via overlap of their rod end segments [2,3,9,13,14]. During nuclear assembly, *A*- and *B*-type lamins have different spatial distributions through distinct signal pathways [15,16]. In the early stages of lamina assembly, lamin *B*1 localizes to the nuclear periphery and quickly establishes high-order polymers, whereas lamin *A* exists as a lower-order structure and is only gradually incorporated into the lamina [15,16]. The failure of *B*-type lamin assembly at the end of mitosis is linked to apoptosis, suggesting that the proper assembly of nuclear *B*-type lamin is essential for cell vitality [17].

Mutagenesis studies have shown that lamin *B*1 is essential to maintain nuclear shape. Defective lamin *B*1 causes irregular nuclear shape, which is directly linked to changes in the heterotypic interactions of lamin *B*1 with other lamins and lamin *B*1 associated proteins within the lamina [18–20]. For example, deletion of the rod domain of lamin B1 had been shown to produce irregular nuclear shape in tissue culture cell [19]. These experiments *in vivo* suggest that lamin *B*1 plays a key structural role in the nuclear envelope [21], but the intrinsic mechanical properties of lamin *B*1 networks remain unknown. Electron microscopy of chemically fixed nuclei reveals that lamin filaments form extremely heterogeneous networks [1]. Therefore, a traditional bulk rheological measurement of the mechanical properties of lamin networks is inadequate.

In this study, we used particle tracking methods and differential interference contrast (DIC) microscopy to examine the micromechanical response and the ultrastructural distribution of lamin *B*1 networks *in vitro*. Our results show that lamin *B*1 can, even in the absence of auxiliary proteins, form stiff, solidlike, and yet extremely porous structures that are well suited to provide structural strength to the nuclear lamina. To determine the local variations in lamin density in the network and to rigorously extract local viscoelastic moduli from the mean-squared displacement profiles of non-

*Corresponding author. Email address: yiider@jhu.edu

interacting particles, we exploit various surface chemistries of the probe microspheres. These include amine-modification, carboxylation, and polyethylene glycol–modification of the microsphere surface. Combining DIC microscopy and particle tracking microrheology allows us to relate the local organization of a material to its local mechanical properties.

II. METHODS AND MATERIALS

Lamin *B*1 purification and assembly

Unless specified otherwise, all reagents are purchased from Sigma (St. Louis, MO). Human lamin *B*1 cDNA was a generous gift from Dr. E.C. Schirmer (The Scripps Research Institute, San Diego, CA). Lamin *B*1 purification follows protocols described in Refs. [12,19]. In brief, human lamin *B*1 cDNA construct was transformed into *E. coli* strain BL21/DE3 (Stratagene, La Jolla, CA) and the transformed *E. coli* was grown at 37 °C in SOB medium supplemented with 50 μg/mL kanamycin. Expression was induced with 1 mM isopropyl-β-*D*-thiogalactopyranoside (IPTG) at $\mathrm{O.D.}_{595}$ about 0.7 for 4 h at 37 °C. Cells were lysed by sonication in phosphate buffer saline (PBS) with 1.5 mM β-mercaptoethanol and protease inhibitor. After a 7-min centrifugation at 10 000 g, the pellet was washed with 0.2% Triton X-100 and resuspended in 20 mM Tris, pH 8.0, 300 mM NaCl, 8 M urea, 3 mM β-mercaptoethanol, 0.2 mM phenylmethyl sulphonyl fluoride (PMSF). The solution was then incubated with Ni-NTA resin (Qiagen, Gaithersburg, MD) for 45 min and eluted in fractions with the same buffer containing a 0–200 mM imidazole gradient. The eluate was dialyzed in 20 mM Tris, pH 8.0, 8 M urea, 3 mM β-mercaptoethanol, 0.2 mM PMSF and was applied to a mono-Q column (Bio-Rad, Hercules, CA), eluted with NaCl gradient from 0 to 1 M. The lamin-rich fraction was examined by SDS-PAGE and further dialyzed into 20 mM Tris, pH 8.0, 8 M urea, 2 mM DTT, 0.2 mM PMSF for storage. Protein purity was verified to be $>99\%$ by SDS-PAGE following densitometry.

For filament assembly, lamin in 8 M urea at 1 mg/mL was dialyzed against 20 mM Tris, pH 8.8, 1 mM EDTA, 1 mM DTT, 0.2 mM PMSF [19] for 16 h at 4 °C. Prior to the experiment, 150 mM NaCl was added to the solution to induce lamin assembly. Alternatively, dialysis in steps, which is, for instance, required for keratin [22], did not affect the structural and mechanical outcomes of lamin *B*1 networks (data not shown).

Network heterogeneity and microrheology assessed by multiple-particle tracking

We probed the micromechanical properties and heterogeneity of lamin *B*1 networks using multiple-particle tracking microrheology first introduced by Apgar *et al.* [23]. The trajectories of 1-μm-diam polystyrene (PS), fluorescent microspheres (Molecular Probes, Eugene, OR) imbedded in lamin *B*1 solutions were recorded using a silicon-intensified transmitter (SIT) camera (Dage-MTI, Michigan City, IN) mounted on an inverted fluorescence microscope equipped with a 100-X oil-immersion lens (N.A. 1.3) (Nikon, Melville, NY) [23,24]. The intensity-weighted centroid of each microsphere was tracked with $\sim$5 nm resolution, as determined by immobilizing similar microspheres on a glass coverslip using a strong adhesive and tracking their apparent displacements [23]. Fields of view were selected randomly within each specimen and, for each tested lamin concentration, trajectories of 150–200 microspheres were recorded.

Images of the microspheres were captured at a frequency of 30 frame/s for 20 s using a custom routine incorporated to the image-acquisition system Metamorph (Universal Imaging Corp., West Chester, PA) [25]. From the time-dependent coordinates of the microspheres centroids, $[x(t),y(t)]$, time-averaged mean-squared displacements (MSD) were calculated, $\langle \Delta r^2(\tau)\rangle = \langle [x(t+\tau)-x(t)]^2+[y(t+\tau)-y(t)]^2\rangle$, where t is the elapsed time and τ is the time scale or time lag. MSD profiles were then transformed into effective viscoelastic moduli as described [26,27]. The distribution of MSD profiles of $\sim$150 microspheres was statistically characterized as described by Tseng *et al.* [28]. All multiple-particle tracking measurements were conducted at 25 °C.

Preparation of PEGylated microspheres

To probe the local micromechanical properties of lamin gels from MSD profiles, we used polyethylene glycol (PEG) coated (PEGylated) microspheres. 5 mg/mL amine-terminated PEG (diamino-PEG, average MW 3400) (Shearwater, Huntsville, AL) in 50 mM MES, pH 6.0 was mixed at a 1:1 ratio with a 2% w/v aqueous suspension of carboxylated-modified PS microspheres (Molecular Probes, Eugene, OR) and incubated for 15 min at room temperature. 1-ethyl-3-(3-dimethylaminopropyl)-carbodiimide (EDAC) was then added to a final concentration of 4 mg/mL and the pH of the solution was adjusted to 6.5. The solution was then incubated overnight. To quench the reaction, 100 mM glycine was added; the mixture was incubated for 30 min at room temperature. PEGylated microspheres were collected by centrifugation (3300 g for 15 min) and washed three times with PBS. The suspension was stored at 4 °C.

Differential-interference-contrast microscopy

Differential-interference-contrast (DIC) microscopy (Nikon) was used to visualize large polymer microstructures [29]. Images were acquired by a charged-coupled-device (CCD) camera (Orca II, Hammamatsu, Bridgewater, NJ), which was controlled by the Metamorph/Metaview imaging system. Approximately 100–200 μL of 3 mg/mL lamin *B*1 solution was used in a 500-μL well to obtain clear images of lamin networks.

III. RESULTS

Microstructure of lamin *B*1 networks

To relate structure to mechanical function, lamin *B*1 networks were visualized by DIC microscopy and their local mechanical properties were probed by multiple-particle tracking microrheology. Similarly to IF keratin and vimentin

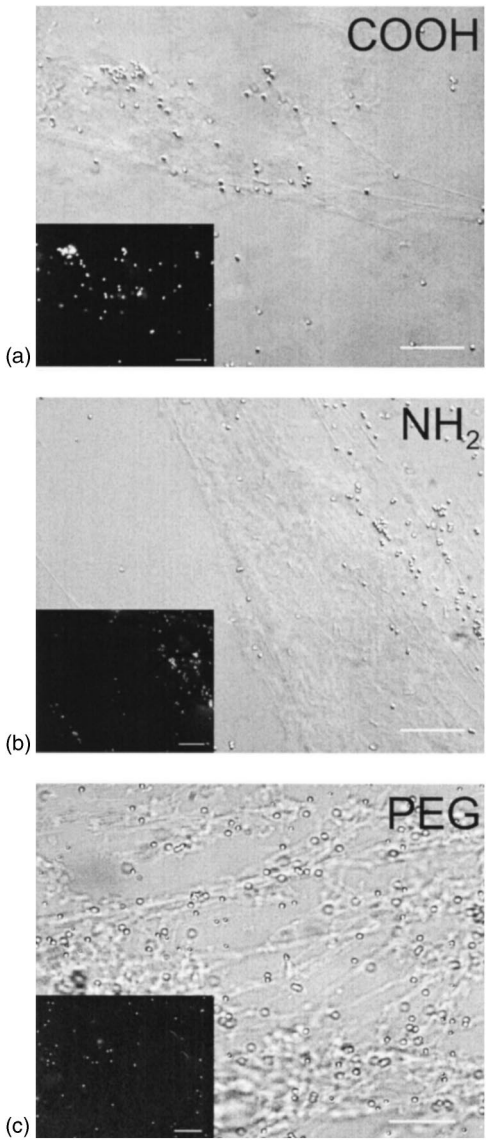

FIG. 1. Microstructure of lamin *B*1 suspensions marked with fluorescent amine-modified and carboxylated microspheres. Lamin *B*1 networks (3 mg/mL) in polymerization buffer at 25 °C. Scale bar, 10 μm. (a) Carboxylated microspheres. (b) Amine-modified microspheres. (c) PEGylated microspheres. Microspheres embedded in lamin-rich regions remain in focus, while microspheres in lamin-poor regions are somewhat fuzzy because of Brownian motion. Panels (a)–(c) are differential interference contrast (DIC) micrographs. **Insets** in panels (a)–(c) are micrographs of the fluorescently labeled microspheres embedded in those lamin *B*1 suspensions. The microspheres have a diameter of 1 μm.

suspensions exposed to high pH or high NaCl concentrations [29,30], DIC microscopy detected the formation of large lamin *B*1 aggregates and bundles (Fig. 1) surrounded with regions seemingly depleted in lamin. By adjusting the focal plane, these bundles were often seen as three-dimensional arrays that extended beyond 100 μm, implying that they arise from association of lamin filaments [19].

Fluorescence microscopy combined with DIC microscopy revealed that amine-modified and carboxylated PS microspheres primarily colocalized with the regions rich in lamin networks suspension [Figs. 1(a) and 1(b) and respective insets]. The spontaneous thermally excited motion of microspheres (diameter 1 μm) embedded in lamin-rich regions was monitored in real time with 33-ms temporal resolution and 5-nm spatial resolution using the multiple-particle tracking approach [23]. From the trajectories of the microspheres' centroids [Figs. 2(a) and 2(b)], mean-squared displacements (MSD) were computed [Figs. 2(c)–2(e)]. A minority of carboxylated and amine-modified microspheres showed unrestricted motion [Fig. 2(a)] with an MSD growing linearly with time [top curves in Figs. 2(c) and 2(d)], indicative of viscous diffusion. However, the motion of the majority of amine-modified and carboxylated microspheres was extremely restricted [Fig. 2(b)], e.g., the microspheres' transport was mostly subdiffusive with an MSD growing much more slowly than time [bottom curves in Figs. 2(c) and 2(d)]. These results suggest that most microspheres were trapped in the lamin *B*1 network, possibly due to entropic (i.e., steric) caging by the overlapping lamin filaments and/or nonsteric interactions between the microspheres and lamin.

The proportion of carboxylated and amine-modified microspheres showing restricted motion was much higher than those undergoing viscous diffusion [Fig. 3(a)]. Therefore, lamin *B*1 networks organize into heterogeneous networks containing lamin-rich regions and lamin-poor regions.

Local and global heterogeneity of lamin *B*1 networks

To reduce interactions between microspheres and lamin filaments and probe the local mechanical properties of lamin *B*1 gels, we functionalized 1-μm-diam PS microspheres with polyethylene glycol (PEG), a hydrophilic polymer known to interact little with proteins (see Sec. II). PEG-coated (or PEGylated) microspheres dispersed throughout the lamin *B*1 suspensions, in regions rich and depleted in lamin *B*1, as assessed by combining DIC microscopy of the lamin gels and fluorescence microscopy of the microspheres [Fig. 1(c) and inset]. Unlike amine-modified and carboxylated microspheres, we observed no enrichment of PEGylated microspheres in lamin-rich regions [Fig. 1(c) and inset]. The proportion of PEGylated microspheres in lamin-rich and lamin-poor regions was similar [Fig. 3(a)].

The random movements of hundreds of individual PEGylated microspheres were monitored and statistically analyzed to quantify the network's degree of heterogeneity and its microrheology (see Sec. II). The MSD profiles of PEGylated microspheres can be organized into two distinct families [top and bottom curves in Fig. 2(e)]. MSD profiles either grew linearly with time [top curves in Fig. 2(e)], a signature of viscous diffusion, or grew much more slowly than time [bottom curves in Fig. 2(e)], a signature of viscoelastic trapping of the microspheres by the surrounding network. Accordingly, the distribution of MSD values at a fixed time scale (0.1 s) displayed two maxima [Fig. 3(c) and inset], corresponding to the groupings of MSD profiles into low and high values.

To quantify the global heterogeneity of the network as well as the local heterogeneity of lamin-rich and lamin-poor regions, MSD values ($n=250$) were rank-ordered and the

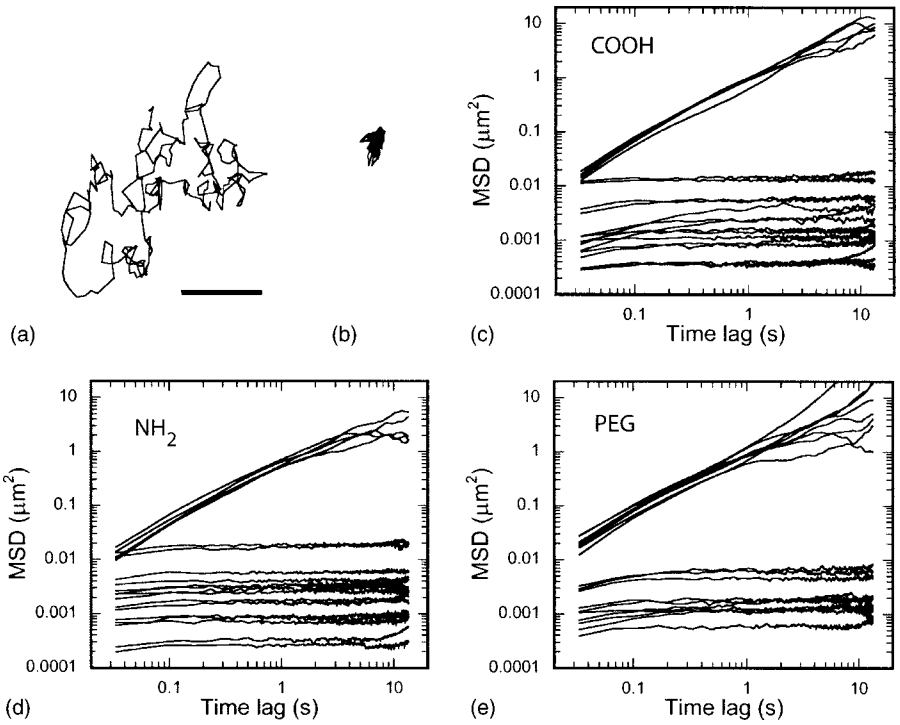

FIG. 2. Tracking the spontaneous movements of amine-modified and PEGylated microspheres in lamin *B*1 networks. Lamin *B*1 networks (3 mg/mL) in polymerization buffer at 25 °C for 60 min. (a) Typical trajectory of a freely moving amine-modified microsphere in a lamin-poor region of the network. (b) Typical trajectory of an amine-modified microsphere embedded in a lamin-rich region of the network. (c) Typical MSD profiles, $\langle \Delta r^2(\tau) \rangle$ vs τ, of amine-modified microspheres in lamin *B*1. (d) Typical MSD profiles of carboxylated microspheres. (e) Typical MSD profiles of PEGylated microspheres. All microspheres have a diameter of 1 μm.

10%, 25%, and 50% highest values were compared to the mean MSD. These markers should exactly be equal to 10%, 25%, and 50% for a perfectly homogeneous material, for which all MSD should be similar, a result indeed verified to hold for glycerol [Fig. 3(b)] [31]. As expected from the apparent heterogeneity of lamin *B*1 gels (Fig. 1), the values of these markers for the entire network were much higher than the homogeneous values of 10%, 25%, and 50% [Fig. 3(b)]. Accordingly, these heterogeneity markers were consistently high for the lamin-rich regions while those for lamin-poor regions were low and close to those of the homogeneous liquid glycerol [Fig. 3(b)].

Micromechanical properties of lamin *B*1 networks using noninteracting microspheres

Local, frequency-dependent viscoelastic moduli of lamin *B*1 networks were directly computed from time-dependent MSD profiles following Mason *et al.* [32]. The elastic modulus calculated from the linear MSD profiles corresponding to lamin-poor regions [top curves in Fig. 2(e)] was too small to be calculated. However, the viscous modulus was measurable and increased (almost) linearly with frequency (data not shown), a signature of purely viscous liquidlike behavior. The corresponding dynamic viscosity ($\eta' = G''/\omega$) was $\sim 2 \times 10^{-3}$ Pa s (2 centiPoise), which is approximately twice as high as the viscosity of buffer. In contrast, the elastic modulus calculated from subdiffusive MSD profiles corresponding to lamin-rich regions was much higher than the viscous modulus, a signature of solidlike behavior [Fig. 4(b)]. Mechanical properties measured using PEGylated microspheres were verified to be independent of the microsphere size.

IV. DISCUSSION

Using particle-tracking methods, we measured the micromechanical and ultrastructural properties of lamin *B*1 networks. Combining DIC microscopy and nanotracking of PEGylated microspheres directly relates the microstructure of a biological material to its local density and mechanical properties. Lamin *B*1 polymers form remarkably solidlike structures. DIC microscopy and particle tracking reveal that lamin *B*1 gels form heterogeneous microstructures that feature lamin-poor pores of interstitial viscosity twice that of a buffer.

DIC and fluorescence microscopy combined with particle tracking reveal the presence of lamin-rich and lamin-poor regions within lamin gels. This combined microscopy reveals that lamin *B*1 gels are extremely porous: ~60% of PEGylated microspheres move subdiffusively within lamin-rich regions. ~40% of PEGylated microspheres move diffusively within lamin-poor regions, regions that are significantly softer than the bulk stiffness of the gel.

Because the MSD of the probe PEGylated microspheres is proportional to time in those lamin-poor regions, $\langle \Delta r^2(\tau) \rangle \sim \tau$, the effective viscosity can be obtained directly from the Stokes-Einstein relation [33], which relates the diffusion coefficient to the size of the microsphere and to the viscosity of the suspending fluid. Here, $\langle \Delta r^2(\tau) \rangle = 4D\tau$, where $D = k_B T / 6\pi a \eta$ is the constant diffusion coefficient of PEGylated microspheres in lamin-poor regions of the gel, k_B is Boltzmann's constant, T is the absolute temperature, and a is the radius of the microsphere. We find a diffusion coefficient of $\sim 0.21\ \mu m^2/s$, corresponding to a viscosity of $\sim 2 \times 10^{-3}$ Pa s (1 Pa s = 10 Poise) (Fig. 5). The diffusion coefficient of the same 1-μm-diam microspheres in water (viscosity 1×10^{-3} Pa s or 1 centiPoise) is $\sim 0.44\ \mu m^2/s$.

The diffusion coefficient of micron- and submicron-sized microspheres in a fluid is by definition the ratio $D = \langle \Delta r^2(\tau) \rangle / 4\tau$ in two dimensions. This diffusion coefficient D is a constant independent of time when the microspheres are immersed in purely viscous liquid (no elasticity). This is

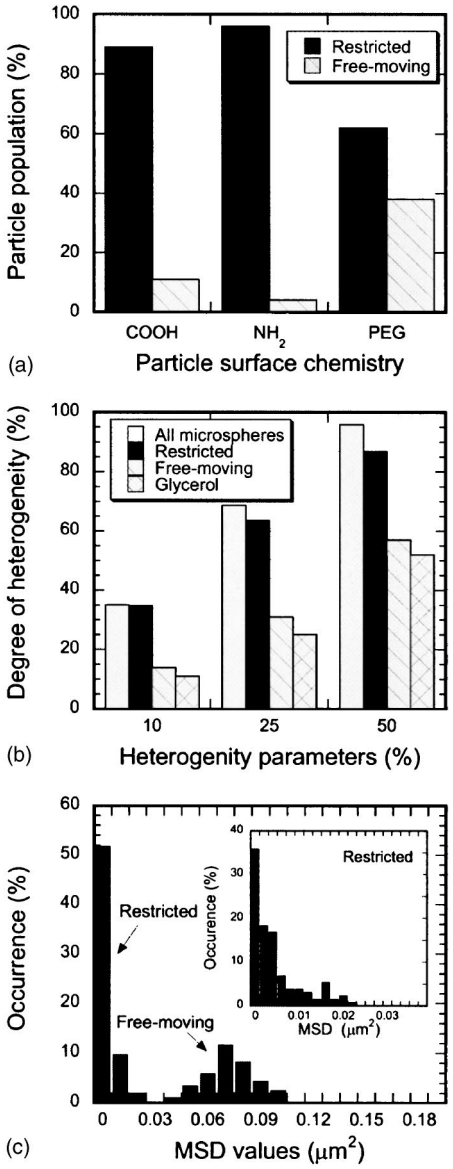

FIG. 3. Lamin *B*1 network heterogeneity assessed by tracking the spontaneous movements of individual carboxylated and PEGylated microspheres. Lamin *B*1 networks (3 mg/mL) in polymerization buffer at 25 °C for 60 min. (a) Proportions of restricted and free-moving microspheres for amine-modified, carboxylated, and PEGylated microspheres in a 3 mg/mL lamin *B*1 solution. (b) Degree of heterogeneity for all (restricted and free-moving) microspheres. These parameters are close to 10%, 25%, and 50% for a homogeneous material like glycerol and progressively higher than those values for more heterogeneous materials. (c) Distribution of MSD's of PEGylated microspheres in a 3 mg/mL lamin *B*1 network at a time scale of 0.1 s. **Inset:** MSD distribution of the microspheres undergoing restricted motion. All microspheres have a diameter of 1 μm.

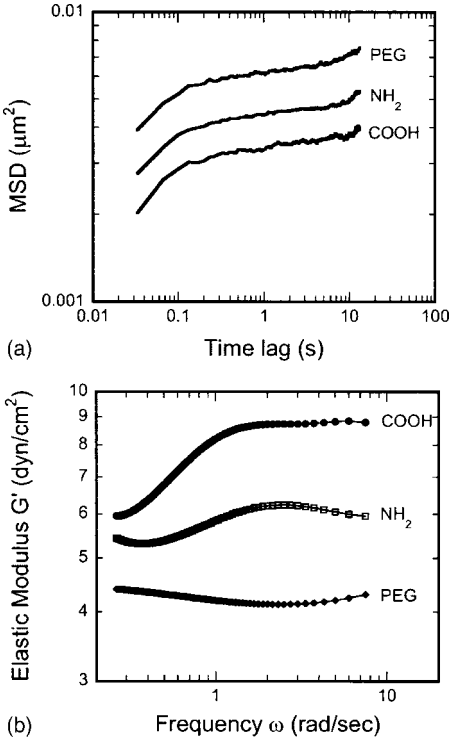

FIG. 4. Ensemble-averaged MSD of microspheres embedded in lamin *B*1 suspensions and apparent microelastic moduli from MSD profiles. Lamin *B*1 networks (3 mg/mL) in polymerization buffer at 25 °C for 60 min. (a) Ensemble-averaged MSD profiles for different types of microspheres embedded in lamin-rich regions of a 3 mg/mL lamin *B*1 network. (b) Frequency-dependent elastic modulus, $G'(\omega)$, of lamin *B*1 networks calculated from the ensemble-averaged MSD of the PEGylated microspheres embedded in the lamin-rich regions of the gel. The mathematical transformation of MSD profiles into $G'(\omega)$ is detailed in Refs. [27,32].

the case of 1-μm PEGylated microspheres diffusing in lamin-poor regions (Fig. 5, top curve); it is also the case of PEGylated microspheres diffusing in water or glycerol. However, the diffusion coefficient of microspheres imbedded in a viscoelastic fluid is not a constant. To understand this effect, consider first the case of a perfectly elastic material like a stiff rubber. Each time a microsphere moves in a direction, due to its kinetic energy imparted by the thermal energy k_BT, that microsphere is subject to a restoring force (no dissipation) created by the surrounding elastic medium. This restor-

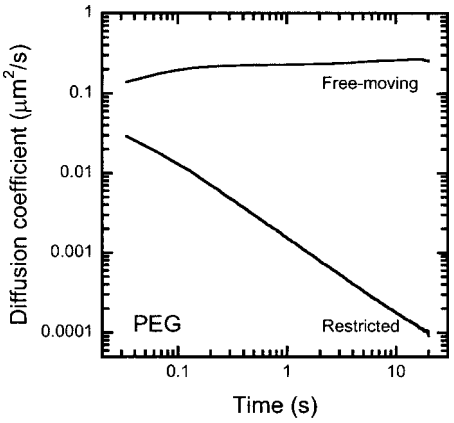

FIG. 5. Diffusion coefficient of PEGylated microspheres embedded in lamin *B*1 gels. Mean diffusion coefficient of 1-μm-diam PEGylated PS microspheres suspended in lamin-poor regions of the gel (top curve) and embedded in lamin-rich regions (bottom curve).

ing force takes the microsphere back to its original position. The MSD of such microspheres is a constant, $\langle \Delta r^2(\tau) \rangle = C$, and therefore the diffusion coefficient, $D = \langle \Delta r^2(\tau) \rangle / 4\tau = C/\tau$, is inversely proportional to time. For a viscoelastic medium, which is both viscous and elastic, such as the filament-rich regions of a lamin *B*1 gel, *D* adopts an intermediate temporal profile, where *D* is neither constant nor inversely proportional to τ (Fig. 5, bottom curve).

The viscosity experienced by the microspheres in the lamin-poor region is higher than that of the buffer ($\sim$1 centiPoise). This result suggests that the pores contain a non-negligible concentration of lamin. One can label this viscosity as an "interstitial" viscosity [34] that describes the viscosity of the lamin-poor region, which interdigitates into thick and elastic lamin-rich regions. The Stokes-Einstein analysis described above does not hold in lamin-rich regions of the gel because the MSD does not scale linearly with time. For PEGylated microspheres embedded on those regions, the diffusion coefficient is not a constant, and Mason *et al.*'s analysis [32], which takes into account the partial elastic trapping of the microsphere, is required to extract local elasticity and viscosity.

Despite the lamin-rich and lamin-poor regions defining the heterogeneity of the lamin gels, further statistical analysis of particle tracking data in these two subgroups shows that the high degree of heterogeneity of lamin networks stems from the lamin-rich regions. The degree of heterogeneity of lamin-poor regions is low and resembles that of glycerol, a viscous liquid that can be considered to be homogeneous at length scales comparable to the diameter of the microspheres. In contrast, the degree of heterogeneity of the filament-rich regions in lamin *B*1 gels is almost as high as that obtained by combining all particle tracking data. The degree of heterogeneity of lamin *B*1 gels is also much higher than observed in concentrated solutions of *F*-actin networks without *F*-actin crosslinkers [35], but as high as in *F*-actin networks in the presence of the *F*-actin crosslinking/bundling proteins α-actinin [25,28,36–39], fascin [23,40], and filamin [41].

Combining DIC microscopy and particle tracking microrheometry allows us to relate *directly* the local organization of a material to its local mechanical properties. Since its introduction [32,42], particle tracking microrheology has been used extensively to probe the local viscoelasticity of reconstituted cytoskeleton networks [25,30,42–45] and DNA solutions [31,32], the nucleus [21] and cytoplasm [26,46] of living cells, and the micromechanics of complex materials [32,43,47,48]. This paper has introduced an analysis that establishes the structure-function of a complex material in a single experiment. The same method can now be extended to living cells. Here, particle tracking of fluorescently labeled particles of one color is to be combined with fluorescence microscopy of subcellular structures or proteins labeled with another fluorescent dye. For instance, lamin organization in the interphase nucleus and associated microrheology would be obtained with GFP-lamin and PEGylated red fluorescent microspheres [21].

ACKNOWLEDGMENTS

We thank Dr. E.C. Schirmer (The Scripps Research Institute, CA) for his generous gift of human lamin *B*1 cDNA. This work was funded by the NSF (NES/NIRT CTS0210718) and NASA (NAG9-1563).

[1] U. Aebi *et al.*, Nature (London) **323**, 560 (1986).
[2] E. Heitlinger *et al.*, J. Struct. Biol. **108**, 74 (1992).
[3] N. Stuurman, B. Sasse, and P. A. Fisher, J. Struct. Biol. **117**, 1 (1996).
[4] T. H. Hoger *et al.*, Chromosoma **100**, 67 (1990).
[5] M. Zewe *et al.*, Eur. J. Cell Biol. **56**, 342 (1991).
[6] R. P. Aaronson and G. Blobel, Proc. Natl. Acad. Sci. U.S.A. **72**, 1007 (1975).
[7] R. D. Moir, T. P. Spann, and R. D. Goldman, Int. Rev. Cytol. **162B**, 141 (1995).
[8] M. R. Paddy *et al.*, Cell **62**, 89 (1990).
[9] C. Gieffers and G. Krohne, Eur. J. Cell Biol. **55**, 191 (1991).
[10] R. D. Moir *et al.*, J. Cell Biol. **149**, 1179 (2000).
[11] J. Newport and T. Spann, Cell **48**, 219 (1987).
[12] A. Karabinos *et al.*, J. Mol. Biol. **325**, 241 (2003).
[13] S. Heins and U. Aebi, Curr. Opin. Cell Biol. **6**, 25 (1994).
[14] E. Heitlinger *et al.*, J. Cell Biol. **113**, 485 (1991).
[15] R. D. Moir *et al.*, J. Struct. Biol. **129**, 324 (2000).
[16] R. D. Moir *et al.*, J. Cell Biol. **151**, 1155 (2000).
[17] R. L. Steen and P. Collas, J. Cell Biol. **153**, 621 (2001).
[18] R. Foisner and L. Gerace, Cell **73**, 1267 (1993).
[19] E. C. Schirmer, T. Guan, and L. Gerace, J. Cell Biol. **153**, 479 (2001).
[20] K. Furukawa, C. E. Fritze, and L. Gerace, J. Biol. Chem. **273**, 4213 (1998).
[21] Y. Tseng *et al.*, J. Cell. Sci. **117**, 2159 (2004).
[22] S. Yamada, D. Wirtz, and P. A. Coulombe, J. Struct. Biol. **143**, 45 (2003).
[23] J. Apgar *et al.*, Biophys. J. **79**, 1095 (2000).
[24] P. Leduc *et al.*, Nature (London) **399**, 564 (1999).
[25] Y. Tseng and D. Wirtz, Biophys. J. **81**, 1643 (2001).
[26] Y. Tseng, T. P. Kole, and D. Wirtz, Biophys. J. **83**, 3162 (2002).
[27] T. P. Kole *et al.*, Mol. Biol. Cell **15**, 3475 (2004).
[28] Y. Tseng, K. M. An, and D. Wirtz, J. Biol. Chem. **277**, 18 143 (2002).
[29] S. Yamada, D. Wirtz, and P. A. Coulombe, Mol. Biol. Cell **13**, 382 (2002).
[30] L. Ma *et al.*, Nat. Cell Biol. **3**, 503 (2001).
[31] A. Goodman, Y. Tseng, and D. Wirtz, J. Mol. Biol. **323**, 199 (2002).
[32] T. G. Mason *et al.*, Phys. Rev. Lett. **79**, 3282 (1997).
[33] H. C. Berg, *Random Walks in Biology* (Princeton University Press, Princeton, NJ, 1993).
[34] K. Luby-Phelps *et al.*, Proc. Natl. Acad. Sci. U.S.A. **84**, 4910 (1987).
[35] A. Palmer *et al.*, Biophys. J. **76**, 1063 (1999).
[36] J. Xu, D. Wirtz, and T. D. Pollard, J. Biol. Chem. **273**, 9570

(1998).
[37] J. Xu, Y. Tseng, and D. Wirtz, J. Biol. Chem. **275**, 35 886 (2000).
[38] A. Palmer, J. Xu, and D. Wirtz, Rheol. Acta **37**, 97 (1998).
[39] Y. Tseng *et al.*, J. Biol. Chem. **277**, 25609 (2002).
[40] Y. Tseng *et al.*, J. Mol. Biol. **310**, 351 (2001).
[41] Y. Tseng *et al.*, J. Biol. Chem. **279**, 1819 (2004).
[42] F. Gittes *et al.*, Phys. Rev. Lett. **79**, 3286 (1997).
[43] B. Schnurr *et al.*, Macromolecules **30**, 7781 (1997).
[44] J. L. McGrath, J. H. Hartwig, and S. C. Kuo, Biophys. J. **79**, 3258 (2000).
[45] J. Xu, A. Palmer, and D. Wirtz, Macromolecules **31**, 6486 (1998).
[46] S. Yamada, D. Wirtz, and S. C. Kuo, Biophys. J. **78**, 1736 (2000).
[47] J. Xu *et al.*, Biomacromolecules **3**, 92 (2002).
[48] W. A. Petka *et al.*, Science **281**, 389 (1998).